2014-04-16

A Carbon Nanotube-Based Raman-Imaging Immunoassay for Evaluating Tumor Targeting Ligands

UTD AUTHOR(S): Pooja Bajaj, Carole Mikoryak, Ruhung Wong, David K. Bushdiecker II, Pauras Memon, Rockford K. Draper, Gregg R. Dieckmann, Paul Pantano and Inga H.Musselman.

Analyst

PAPER

View Article Online
View Journal | View Issue

A carbon nanotube-based Raman-imaging immunoassay for evaluating tumor targeting ligands†

Cite this: *Analyst*, 2014, **139**, 3069

Pooja Bajaj,[a] Carole Mikoryak,[b] Ruhung Wang,[ab] David K. Bushdiecker II,[a] Pauras Memon,[a] Rockford K. Draper,[abc] Gregg R. Dieckmann,[ac] Paul Pantano[ac] and Inga H. Musselman*[ac]

Received 5th February 2014
Accepted 16th April 2014

DOI: 10.1039/c4an00258j

www.rsc.org/analyst

Herein, we describe a versatile immunoassay that uses biotinylated single-walled carbon nanotubes (SWNTs) as a Raman label, avidin–biotin chemistry to link targeting ligands to the label, and confocal Raman microscopy to image whole cells. Using a breast tumor cell model, we demonstrate the usefulness of the method to assess membrane receptor/ligand systems by evaluating a monoclonal antibody, Her-66, known to target the Her2 receptors that are overexpressed on these cells. We present two-dimensional Raman images of the cellular distribution of the SWNT labels corresponding to the distribution of the Her2 receptors in different focal planes through the cell with validation of the method using immunofluorescence microscopy, demonstrating that the Her-66–SWNT complexes were targeted to Her2 cell receptors.

Introduction

Targeted therapies are designed to selectively deliver a therapeutic agent to a specific molecular target, thereby providing a more effective treatment with fewer side effects. They are now incorporated in the treatment strategy of many common malignancies including breast, colorectal, lung, and pancreatic cancers, as well as lymphoma, leukemia, and myeloma.[1] Recently, the efficacy of targeted therapies has improved through the use of nanoparticles that can package drugs with a controlled size, shape, and surface chemistry to enhance their solubility, bioavailability, and residence times.[2] An ancillary benefit of using nanoparticles is that many can additionally serve as an imaging label (*e.g.*, a Raman or MRI contrast agent) and as an intrinsic therapeutic agent (*e.g.*, a material that absorbs electromagnetic radiation, converts it to heat, and ablates the cell containing it).

Single-walled carbon nanotubes (SWNTs) are one class of multifunctional nanoparticles that have shown great promise for the imaging and treatment of diseases.[3–6] A SWNT can be represented as a graphene sheet of sp^2-hybridized carbon atoms seamlessly wrapped into a cylindrical tube. SWNT diameters are typically 0.7 to 1.5 nm, lengths range from 10 nm to several centimeters, and the electronic structure can be metallic or semi-conducting depending on how the graphene sheet is rolled up.[7–10] Carboxylated SWNTs (C-SWNTs) are particularly well suited for biomedical applications since functional groups on the nanotube surface facilitate the covalent attachment of targeting agents to ensure that the agents remain associated with the SWNT in complex biological environments. Indeed, there are numerous *in vitro* and *in vivo* studies that report the therapeutic effectiveness of covalently-functionalized SWNT constructs with minimal acute toxicity.[4,6,11–17] Furthermore, in contrast to metal nanoparticles, C-SWNTs have been shown to be biodegraded by neutrophils *in vivo*.[15]

Numerous assays are required to accurately evaluate the effectiveness of a targeted therapy, which depends on many factors including the optimal dose, stability, specificity, toxicity, and degree of cellular internalization.[2] Many of these assays utilize immunofluorescence detection after the targeting agent is labeled with a fluorescent dye. However, in many cases, dye photobleaching limits the use of these assays to short-duration experiments. In contrast, SWNTs make excellent spectroscopic labels because they exhibit persistent Raman scattering, and they are resistant to photobleaching. For example, Cao *et al.* recently demonstrated an immunoassay detection scheme that used SWNTs as a Raman label.[18] In brief, they adsorbed biotin to the SWNTs and used an avidin–biotin coupling scheme to link the SWNTs to an antibody. Then, SWNT resonances observed in Raman spectra collected from cell extracts of cytomegalovirus-infected fibroblasts were used to detect a primary

[a]*Department of Chemistry, The University of Texas at Dallas, Richardson, TX 75080-3021, USA. E-mail: imusselm@utdallas.edu*

[b]*Department of Molecular and Cell Biology, The University of Texas at Dallas, Richardson, TX 75080-3021, USA*

[c]*The Alan G. MacDiarmid NanoTech Institute, The University of Texas at Dallas, Richardson, TX 75080-3021, USA*

† Electronic supplementary information (ESI) available. See DOI: 10.1039/c4an00258j

antibody and a protein antigen with excellent specificity and sensitivity. However, imaging whole cells and knowing the cellular distribution of an antibody targeting agent is required to better understand the mechanisms of cellular binding and/or internalization. This is especially important when the antibody is targeted to a membrane receptor overexpressed on a tumor cell. For example, a number of breast cancer therapies involve targeting the human epidermal growth factor receptor 2 (Her2), a transmembrane tyrosine kinase active glycoprotein linked to breast tumor aggressiveness and pathogenesis,[19,20] using anti-Her2/erB-2 monoclonal antibodies.[21–23]

Today, advances in laser scanning confocal Raman microscopy make it possible to rapidly scan large areas and collect a complete Raman spectrum at every pixel in the image such that cells can be analyzed in a matter of minutes. This technique has been used by our group[13] and others[24] to image the cellular binding and degree of internalization of antibody–SWNT conjugates *in vitro*; furthermore, instruments modified for deep tissue imaging have been used to monitor the accumulation of antibody–SWNT conjugates in tumors *in vivo*.[25] The capabilities of these instruments make them ideally suited to evaluate the efficacy of a SWNT-based therapeutic. For example, we recently used confocal Raman imaging to reveal that antibody–SWNT conjugates internalized by tumor cells were more effective therapeutic agents than those bound to the surface of tumor cells.[13]

Herein, we expand upon the work of Cao *et al.*[18] and present a versatile whole-cell Raman imaging immunoassay that can evaluate the binding and/or internalization of a tumor targeting agent using SWNTs as a Raman label. As a demonstration of the method, we evaluated the cellular distribution of Her2 receptors on BT-474 breast tumor cells using Her-66, a monoclonal antibody that binds Her2 receptors. Once bound to Her2 receptors, a biotinylated secondary antibody is then introduced to bind the primary antibody and to provide biotin groups that can link biotinylated C-SWNTs to the secondary antibody *via* a NeutrAvidin™-FITC bridge (Schemes 1 and 2). This approach enables the binding of the targeted C-SWNTs to Her2 receptors to be validated by imaging the distribution of Her2 receptors on BT-474 cells *via* immunofluorescence microscopy of NeutrAvidin™-FITC and directly detecting the SWNTs associated with the cells *via* laser scanning confocal Raman microscopy.

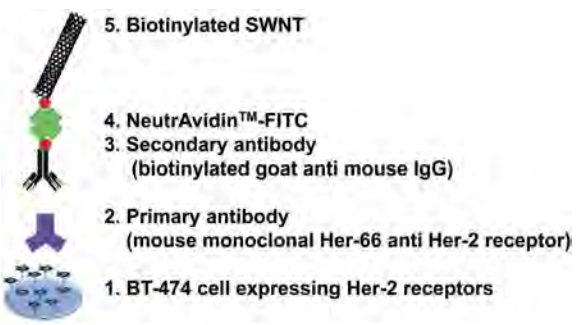

Scheme 1 Schematic diagram of the immunoassay for the binding of a biotinylated SWNT (B-SWNT) to a breast tumor (BT-474) cell. The specific binding of the mouse monoclonal Her-66 antibody to Her2 receptors on the BT-474 cells is followed by the introduction of a biotinylated secondary antibody that binds to the B-SWNT *via* a biotin–avidin–biotin bridge.

Materials and methods

(i) Synthesis of biotinylated SWNTs

In brief, SWNTs were oxidized by nitric acid reflux to form C-SWNTs, which were covalently coupled to a tether of (+)-biotinyl-3,6,9-trioxaundecanediamine (biotin-LC-PEO-amine) to form biotinylated-SWNTs (B-SWNTs). Specifically, raw HiPco SWNTs (Lot #R0519, Carbon Nanotechnologies, Inc.) were dispersed in Triton X-100 (TX-100) and refluxed in nitric acid (6 M) for 12 h generating carboxyl groups at the end caps and sidewalls according to a modified procedure involving sonication and centrifugation.[26–28] The resulting C-SWNTs (0.2 mg) were probe sonicated (VWR Branson Sonifier 250 with a 1/8″-diameter probe tip) continuously for 10 min at 10 W in 1 mL of a 0.1 M 2-(*N*-morpholino)ethanesulfonic acid buffer, pH 5.0 (MES, 99.5%, Sigma-Aldrich) in a 1.5 mL Eppendorf tube placed in an ice water bath. To remove C-SWNT bundles and other impurities from the samples, the homogeneous black dispersions were centrifuged at a low speed of 700*g* for 10 min (Eppendorf Centrifuge 5424), the supernatant (950 μL) was recovered, and the pellet was discarded. The supernatant was centrifuged a second time at 16 000*g* for 20 min, and 850 μL of supernatant was collected (the pellet was discarded).

Stock solutions of 1.0 mM biotin-LC-PEO-amine (98%, Pierce Biotechnologies) and 50 mM 1-ethyl-3-(3-dimethylaminopropyl) carbodiimide hydrochloride (EDC, 98%, Pierce Biotechnologies) were prepared by dissolving biotin LC-PEO-amine (0.42 mg) and EDC (9.57 mg) in 1.0 mL of MES buffer. A 2.5 μL aliquot of the biotin LC-PEO-amine solution (2.5 nmol) and a 100 μL aliquot of the EDC solution (5 μmol) were added to the 1.5 mL Eppendorf tube containing C-SWNTs. The mixture was vortexed for 15 s followed by mixing on a rugged rotor Glas-Col (model 099A RD4512) for 2 h at room temperature. The product was centrifuged at 13 000*g* for 20 min at 4 °C (Beckman TL-100 Ultracentrifuge) to remove unreacted EDC and biotin LC-PEO-amine from the resultant B-SWNTs. The supernatant was recovered and dialyzed using a 10 kDa molecular weight cut-off dialysis cartridge (Slide-A-Lyzer, Pierce Biotechnologies) for 3 days against 4 L of deionized (DI) water. The water was changed twice the first day and once each of the remaining days. After dialysis, the B-SWNT dispersions were characterized by atomic force microscopy (AFM), transmission electron microscopy (TEM), UV-Vis-NIR spectrophotometry, and Raman spectroscopy. For cell and receptor-mediated immunoassay binding studies, several B-SWNT dispersions were pooled and concentrated by solvent evaporation. B-SWNT loadings were characterized using sodium dodecyl sulfate-polyacrylamide gel electrophoresis (SDS-PAGE).

(ii) AFM of SWNT dispersions

AFM images were acquired in air under ambient conditions using a Nanoscope III Multimode Scanning Probe Microscope

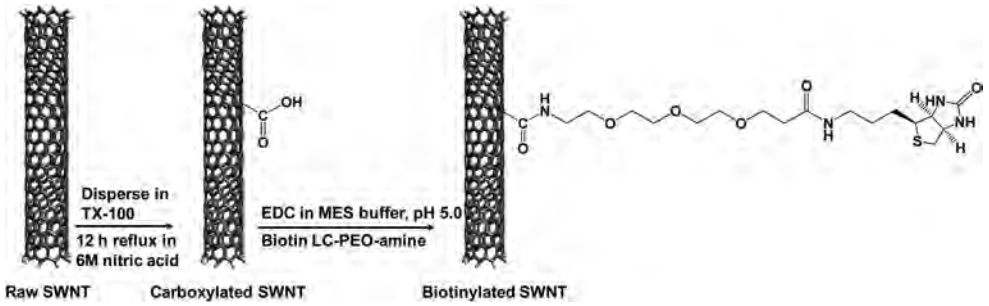

Scheme 2 Schematic diagram of the SWNT carboxylation and biotinylation reactions. HiPco SWNTs dispersed by TX-100 were refluxed in nitric acid to yield carboxylated SWNTs (C-SWNTs), which were reacted with biotin LC-PEO-amine to yield biotinylated SWNTs (B-SWNTs).

operated in the TappingMode™ (Veeco Instruments, Inc.). The AFM piezoelectric "J" scanner was calibrated using a Nano Devices Inc. standard, and the height calibration was verified using hydrofluoric acid etched pits in muscovite mica.[29] AFM images for height analysis were acquired using a reduced *Z*-limit (100–200 V) and silicon cantilevers/tips (force constant 5.0 N m^{-1}, resonant frequency 180 kHz, Veeco Instruments, Inc.).[30] Aliquots (20 μL) of B-SWNTs and C-SWNTs were spun-cast separately onto freshly-cleaved muscovite mica (Asheville-Schoonmaker Mica Co.) at 3500 rpm for 30 s. The samples were dried in a desiccator overnight at room temperature prior to imaging.

(iii) TEM of B-SWNTs labeled with streptavidin gold

TEM images of B-SWNTs tagged with streptavidin-coated gold markers (5 nm diameter, Kirkegaard and Perry Laboratories Inc.) were obtained using a high contrast Tecnai™ FEI G2 Spirit BioTwin transmission electron microscope operated at 120 kV using a LaB_6 emitter. The instrument is equipped with a 2k × 2k Gatan Ultrascan 1000 multiport CCD camera. Nickel grids (200 mesh, Ted Pella) coated with carbon were used as the support for the samples. The B-SWNT dispersion (100 μL) was treated with 5 μL of a 1 : 50 dilution of the streptavidin–gold conjugate in DI water and allowed to react for 12 h at room temperature. Following the reaction, the dispersion was ultracentrifuged (Beckman TL-100 Ultracentrifuge) twice at 47 000*g* for 15 min, and the supernatant containing excess streptavidin–gold conjugate was discarded. The pellet containing streptavidin–gold-labeled B-SWNTs was re-suspended by pipette mixing. The sample (5 μL) was dropped onto a grid, left for 2 min, and the excess was wicked away prior to imaging.

(iv) UV-Vis-NIR spectrophotometry of SWNT dispersions

Background-subtracted absorption spectra of TX-100/SWNTs (control sample in D_2O), C-SWNTs (control sample in D_2O), and B-SWNTs (in DI water) were acquired from 400 to 1400 nm in 1 mm cuvettes (Suprasil 300, Fisher Scientific) using a dual-beam Perkin-Elmer Lambda 900 UV-Vis-NIR spectrophotometer. The spectra were acquired at a scan speed of 125 nm min^{-1} with a 0.5 s integration time.

(v) Raman spectroscopy of SWNT dispersions

Background-subtracted Raman spectra were acquired from C-SWNT and B-SWNT dispersions dried onto glass microscope slides using a WITec alpha 300 series confocal scanning microscope with a 532 nm laser (18 mW) as the excitation source. Wavenumber calibration was performed using the 520.5 cm^{-1} line of a silicon wafer. The spectral resolution was ~1 cm^{-1}. An area of interest viewed with a 20× objective lens was selected with the software, and spectra (average of 3 spectra) were recorded from 100 to 2000 cm^{-1}.

(vi) SDS-PAGE determination of SWNT concentrations in SWNT dispersions

The amounts of C-SWNTs and B-SWNTs used for the binding studies were determined by SDS-PAGE analysis using C-SWNT suspensions as a standard.[31] The C-SWNT standard was prepared by sonicating C-SWNTs (0.2 mg) in 1.0 mL DI water for 10 min at 10 W constant power. The suspensions were not processed further (*i.e.*, centrifuged) before they were used to generate a standard calibration curve. C-SWNT standards and dispersions and B-SWNT dispersions were loaded in increasing volumes into the gel wells. After electrophoresis at 100 V for 2 h, the pixel intensities of the SWNT-containing dark bands at the loading well/stacking gel interface were scanned using a 16-bit flat bed scanner (9520 Photo Scanner, Visioneer) and quantitated using Image Quant software (Image Quant version 5.2, GE Healthcare). The concentrations of SWNTs in C-SWNT and B-SWNT dispersions were determined from a linear fit of the C-SWNT standard calibration curve.

(vii) Breast ductal carcinoma BT-474 cell culture

Breast ductal carcinoma BT-474 cells (American Type Culture Collection, (ATCC), Manassas, VA) were cultured in Hybri-Care culture medium (ATCC) containing 10% fetal calf serum (FCS; HyClone, Logan, UT) and 3.41 g sodium bicarbonate per liter of medium in a 10% CO_2 incubator at 37 °C. The medium was first adjusted to pH 7.2 and then filtered through a 0.2 μm membrane. To determine the number of cells for plating, cells grown in tissue culture dishes were removed with 0.05% trypsin (w/v), and the cell count was determined using a Beckman Coulter Particle Counter (Miami, FL).

(viii) Immunofluorescence microscopy with BT-474 cells

To determine the distribution of the Her2 receptors at 15 °C, the multistep immunoassay (Scheme 1: steps 1 through 4) was performed on live BT-474 cells. Coverslips (12 mm) were pretreated with polylysine to allow for better adhesion of the cells to the glass surface and placed in 4-well tissue culture (TC) dishes. The BT-474 cells were plated at 8×10^4 cells per well on the coverslips, and the cells were grown at 37 °C. Subsequent steps were performed entirely at 15 °C, which slows down the rate of endocytic internalization and keeps epitopes available to the medium while maintaining good adherence of the cells to the substrate. The cells were washed 3 times with phosphate buffered saline (PBS) followed by 10 min incubation in PBS containing 10% FCS to block cell surface non-specific binding sites. The primary antibody, Her-66, containing 1.47 mg mL^{-1} IgG, was diluted 1 : 1000 in 10% FCS, and a volume of 200 μL was placed on each coverslip. The relative binding affinity of the Her-66 antibody on BT474 cells has been reported to be $3.8 \pm 3.2 \times 10^{-9}$ M.[23] This is the concentration necessary to reach 50% saturation of the Her2 receptors. The antibody was allowed to bind for 40 min at the appropriate temperature, followed by washing 3 times with PBS and blocking with 10% FCS for 10 min. As a nonspecific binding control, the primary antibody step was omitted (Scheme 1: steps 1, 3, and 4). The secondary antibody, biotin-conjugated goat anti mouse IgG (Pierce, adjusted to a conc. of 1 μg mL^{-1}), was diluted 1 : 1000 in 10% FCS, and 200 μL was placed on each coverslip and allowed to bind for 40 min. The excess antibody was removed by washing 3 times with PBS and blocked with 10% FCS for 10 min. NeutrAvidin™-FITC (Pierce, 31006 adjusted to a concentration of 5.5 mg mL^{-1}) was diluted 1 : 1250 in 10% FCS. A volume of 200 μL was placed on each coverslip and allowed to bind for 40 min. The unbound NeutrAvidin™-FITC was removed by washing the cells 3 times with PBS. The cells were fixed with cold 4% paraformaldehyde for 20 min, washed 3 times with PBS, and then 3 times with H_2O. The coverslips were mounted on glass microscope slides with Fluoromount-G™ preserved with 0.1% NaN_3 (Southern Biotech) and viewed with a Nikon Eclipse TE-2000U microscope equipped with a Cascade 512B camera and a 60× objective lens (NA = 1.4) (Princeton Instruments). Pixel intensities were adjusted to full-scale, and figures were assembled in Adobe Photoshop 5.5 (Adobe Systems).

(ix) Confocal Raman imaging of the binding of biotinylated SWNTs to BT-474 cells *via* the immunoassay

BT-474 cells treated as described above for the immunofluorescence experiments (Scheme 1: steps 1 through 4) at 15 °C were washed and blocked for 10 min with 10% FBS. The primary antibody, Her-66 (mouse anti Her2 receptors), secondary antibody (biotinylated goat anti-mouse IgG), and NeutrAvidin™-FITC were introduced at the same concentrations as previously described and allowed to bind for 40 min each followed by washing and re-blocking with 10% FCS. B-SWNTs (17.5 μg in 180 μL in 10% FCS) were added to each cover slip and allowed to bind for 40 min (see Scheme 1: step 5). The unbound B-SWNTs were removed by washing once with 10% FCS and 3 times with PBS. The cells were fixed with 4% cold paraformaldehyde (500 μL in each well) at ice bath temperature for 20 min, washed 3 times with PBS, washed with DI water, and dried before analysis by Raman spectroscopy.

The B-SWNTs bound to BT-474 cells *via* the receptor-mediated immunoassay were detected with a WITec alpha 300 series confocal Raman microscope. A minimum of 3 independent Raman images were acquired from a cluster of BT-474 cells (Scheme 1: steps 1 through 5) as well as from control cells (in the absence of primary antibody incubation, *i.e.*, Scheme 1: step 2 omitted). Confocal Raman imaging was typically performed on a 70 × 70 μm area of cells with a 0.3 s integration time for each spectrum (total of 4900 spectra per image). Polynomial background subtraction was carried out on the imaged area. The vertical resolution was 1 μm per pixel and the lateral resolution was 350 nm per pixel. The relative abundance of targeted B-SWNTs on BT-474 cells was determined by adding all CCD counts from the Raman G-band peak (integrated from 1480–1660 cm^{-1}) from each of the 4900 spectra in the image using WITec image analysis software. In addition, a series of images was acquired (integration time of 0.2 s, 6 mW laser power) from a single BT-474 cell over a depth of approximately 8 μm (*z*-step = 0.6 μm) after the cell was treated at 15 °C with primary antibody, biotinylated secondary antibody, NeutrAvidin™-FITC, and B-SWNTs. A reconstructed three-dimensional (3D) image was generated from the G-band region (integrated from 1480–1660 cm^{-1}) of the combined focal stacks using the image analysis software, ImageJ.

Results and discussion

(i) Characterization of C-SWNTs and B-SWNTs

One goal of this work was to create a strong linkage between targeting ligands and the SWNT Raman label. In a fashion similar to the work of Cao *et al.*,[18] we used the versatile avidin–biotin interaction. However, instead of a non-covalent association between a biotinylated surfactant and SWNTs, we employed C-SWNTs to covalently attach biotin to the Raman label. Specifically, TX-100-dispersed HiPco SWNTs were carboxylated by reflux[26,27] for 12 h in nitric acid; the percent carboxylation of the C-SWNTs was determined by X-ray photoelectron spectroscopy (XPS) to be 11% atomic (data not shown).[28] Next, C-SWNTs were covalently coupled to biotin LC-PEO-amine (Scheme 2) using EDC as a catalyst cross-linker, and excess reagents were removed by dialysis. The overall reaction leads to the formation of amide bonds between the primary amines on the biotin LC-PEO-amine and the carboxyl groups on the C-SWNTs to produce biotinylated SWNTs, termed B-SWNTs.

AFM images were acquired from B-SWNTs to study the distribution of biotin LC-PEO-amine moieties (Fig. 1a). The AFM image shows nodules that were not observed in AFM images of C-SWNTs (Fig. S1†), suggesting the presence of biotinylated sites at the ends and sidewalls of the nanotubes. AFM height measurements from bare and coated regions of 18 B-SWNTs were obtained to determine the biotin LC-PEO-amine coating dimensions. The difference between the coated SWNT regions (average height = 3.2 ± 1.5 nm; range 1.5–4.0 nm) and

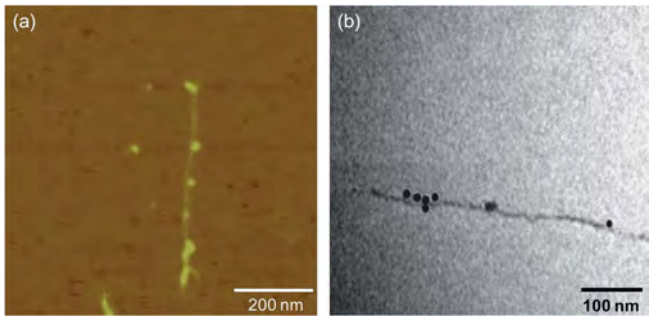

Fig. 1 (a) AFM image (800 × 800 nm) of B-SWNTs where the bright nodules denote the attachment of biotin LC-PEO-amine to C-SWNTs, and (b) TEM image of a streptavidin gold-labeled SWNT-biotin LC-PEO-amine conjugate, where the solid black spheres mark the attachment of streptavidin–gold to biotin sites on the B-SWNT.

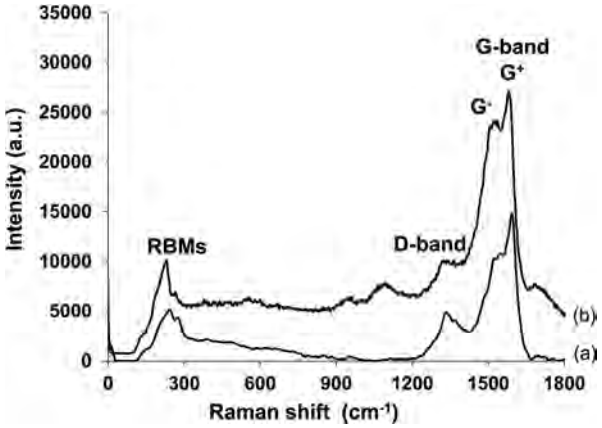

Fig. 2 Raman spectra (laser excitation wavelength 532 nm) of (a) C-SWNTs and (b) B-SWNTs showing characteristic SWNT resonances such as the radial breathing modes (RBMs) between 100–350 cm^{-1}, the disorder D-band at 1350 cm^{-1}, and the tangential G-band at 1585 cm^{-1}.

the bare SWNT regions (average height = 0.9 ± 0.3 nm; range 0.5–1.5 nm) was 2.1 ± 0.6 nm. This thickness closely matches the dimensions of the linker provided by Pierce (biotin LC-PEO-amine dimension = 2.3 nm), and the average height of the bare regions is consistent with the known diameter of individual HiPco SWNTs. Gold nanoparticles (5 nm) coated with streptavidin were reacted with B-SWNTs to visualize the distribution of biotinylated sites along the SWNT structure using TEM (Fig. 1b). The gold labels observed in the TEM image had a similar distribution along the length of the SWNT surface as observed in the AFM image. In summary, the combined AFM and TEM results suggest the presence of biotin groups at SWNT ends and along sidewalls.

UV-Vis-NIR absorption spectrophotometry was used to study the optical transitions of the SWNTs in the NIR region before and after biotinylation. Fig. S2† presents UV-Vis-NIR absorption spectra of TX-100-dispersed raw HiPco SWNTs, C-SWNTs (12 h of nitric acid reflux), and B-SWNTs. The spectrum of TX-100-dispersed SWNTs (Fig. S2a†) shows well-resolved van Hove singularities indicative of debundled, individually dispersed SWNTs,[32] whereas the UV-Vis-NIR spectra of C-SWNTs (Fig. S2b†) and B-SWNTs (Fig. S2c†) show the expected loss of optical features indicative of oxidative modification.[33–38]

SDS-PAGE with optical detection was performed according to the procedure developed by Wang *et al.*[31] to determine the concentrations of SWNTs in C-SWNT and B-SWNT dispersions. Three C-SWNT dispersions were prepared with known amounts of C-SWNTs (0.2 mg C-SWNT powder per mL) that were not subjected to centrifugation following sonication. These C-SWNT dispersions were used to prepare a series of standards for SDS-PAGE. The pixel intensities of the bands from these standards were used to generate a calibration curve from which the concentrations of SWNTs in the purified C-SWNT and B-SWNT dispersions were determined to be 59.5 ± 4.4 ng μL^{-1} and 116.7 ± 4.6 ng μL^{-1}, respectively.

Raman spectroscopy was also performed on C-SWNTs and B-SWNTs. Fig. 2 shows that the Raman spectra of C-SWNTs and B-SWNTs both exhibit characteristic SWNT resonances such as the radial breathing modes (RBMs) (100–350 cm^{-1}), the disorder D-band (1350 cm^{-1}), and the tangential G-band (1585 cm^{-1}). In addition, the G−/G+ line shape of the G-band, characteristic of metallic tubes, was observed in the Raman spectra of both C-SWNTs (Fig. 2a) and B-SWNTs (Fig. 2b).

(ii) Binding of B-SWNTs on BT-474 cells by immunofluorescence and confocal Raman imaging

Immunofluorescence microscopy was conducted to determine the location of Her2 receptors on the surface of BT-474 cells. In these experiments, steps 1–4 of Scheme 1 were performed by incubating cells at 15 °C to slow endocytic internalization of receptors. Fig. 3a demonstrates the binding of NeutrAvidin™-FITC to Her2 receptors on BT-474 cells *via* the linkage provided by the biotinylated secondary antibody and the primary antibody. A representative immunofluorescence imaging stack acquired from a single BT-474 cell over a depth of 8 μm after performing the immunoassay is shown in Fig. S3a.† As the focal plane progressed through the cell, there was modest fluorescence once past the cell surface, consistent with the idea that endocytosis is slow at 15 °C and that the receptors could still be seen on the cell surface. As a control, incubation was carried out while omitting the primary antibody from the immunoassay scheme (skipping step 2 in Scheme 1). In the absence of the primary antibody, only background fluorescence is observed due to insignificant nonspecific binding of NeutrAvidin™-FITC to BT-474 cells (Fig. 3b).

Confocal Raman studies were performed on BT-474 cells following the binding immunoassay with B-SWNTs (Scheme 1: steps 1–5). Fig. 3c and d show optical and 3D Raman images, respectively, of the same BT-474 cell following treatment with the primary antibody, the biotinylated secondary antibody, NeutrAvidin™-FITC, and the B-SWNTs at 15 °C. The bright yellow areas in (d) correspond to G-band intensities (integrated from 1480–1660 cm^{-1}) acquired from each 1 μm^2 pixel in the image. Since cells not exposed to SWNTs did not show any detectable Raman signals in the G-band region (data not shown), the G-band can be used as a direct measure of the

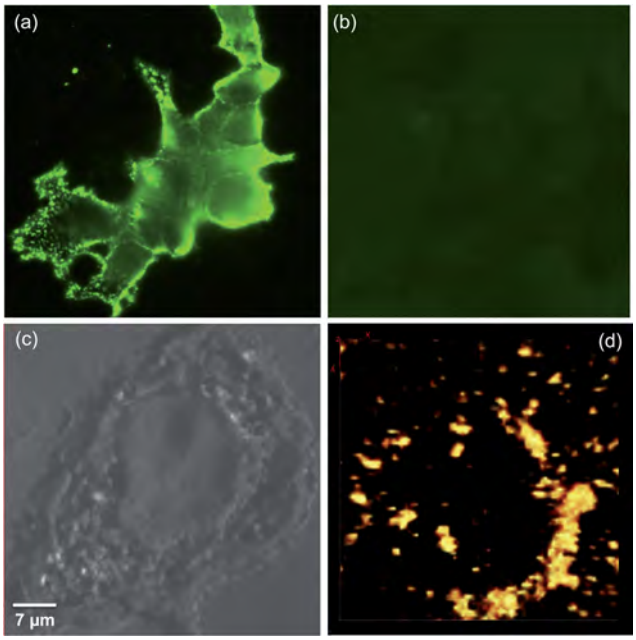

Fig. 3 Immunofluorescence images (normalized to the same color scale) showing (a) the specific binding of NeutrAvidin™-FITC to Her2 receptors on BT-474 cells following treatment with primary antibody, biotinylated secondary antibody, and NeutrAvidin™-FITC at 15 °C, and (b) as a control, the binding of NeutrAvidin™-FITC to Her2 receptors in the absence of the primary antibody at 15 °C. (c) Bright field optical image of the BT-474 cell analyzed. (d) A WITec Alpha 300 scanning confocal microscope was used to acquire 12 two-dimensional Raman images of the same BT-474 cell each at a different focal plane over an approximate 8 μm cell depth with a *z*-step of 0.6 μm following treatment with the primary antibody, the biotinylated secondary antibody, NeutrAvidin™-FITC, and the B-SWNTs at 15 °C. A 3D reconstructed volume was generated from the G-band region of the 12 combined stacks using ImageJ analysis software. The bright yellow areas in (d) correspond to G-band intensities (integrated from 1480–1660 cm^{-1}) acquired from each 1 μm^2 pixel in the image shown on a color intensity scale where yellow is the highest intensity and black is the lowest.

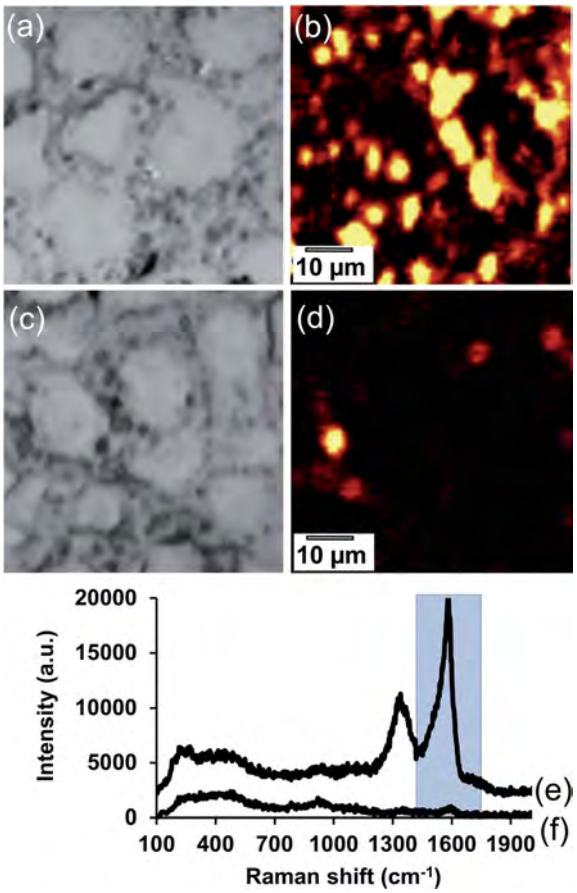

Fig. 4 Optical (a) and Raman (b) images (70 × 70 μm) of the same BT-474 cell cluster following treatment with the primary antibody, the biotinylated secondary antibody, NeutrAvidin™-FITC, and the B-SWNTs at 15 °C. The yellow areas in (b) correspond to G-band intensities (integrated from 1480–1660 cm^{-1}) acquired from each 1 μm^2 pixel in the image. The representative Raman spectrum (e) acquired from the cellular region in (b) displays the characteristic G-band signature of SWNTs. Optical (c) and Raman (d) images (70 × 70 μm) of a different BT-474 cell cluster following the same immunoassay steps at 15 °C except that the primary antibody was omitted (control). The representative Raman spectrum (f) acquired from the cellular region in (d) displays a negligible G-band when the primary antibody is omitted. Spectra (e) and (f) were normalized to the same intensity scale, and images (b) and (d) were normalized to the same color scale.

presence of SWNTs. The similarity in the distribution of labels observed in the immunofluorescence (Fig. 3a) and 3D Raman images (Fig. 3d) indicates that the binding of NeutrAvidin™-FITC to Her2 receptors *via* the linkage between the biotinylated secondary antibody and the primary antibody (Fig. 3a) correlates with the binding of B-SWNTs to Her2 receptors *via* the linkage of the NeutrAvidin™-FITC, biotinylated secondary antibody, and primary antibody (Fig. 3d). A major advantage of confocal Raman imaging is the ability to view different focal planes within a cell. After performing the binding immunoassay, a Raman spectrum was acquired from a cellular region (Fig. S3c†), and a stack of 12 focal images from the cell (Fig. S3b†), each separated by 0.6 μm in the *z*-direction, was assembled in 3D (Fig. 3d) to show the targeting of B-SWNTs for Her2 receptors. The sequential Raman images suggest that B-SWNTs are located on the surface and inside the cells, consistent with slow endocytosis at 15 °C. These results are similar to the immunofluorescence results in Fig. S3a.†

To further demonstrate specificity, additional confocal Raman studies were performed on BT-474 cells at 15 °C following the binding immunoassay with B-SWNTs (Scheme 1: steps 1–5) either with (Fig. 4a and b) or without (Fig. 4c and d) the primary antibody. Fig. 4b again shows an intense Raman G-band signal from the surface binding of B-SWNTs to Her2 receptors on BT-474 cells at 15 °C *via* the linkage provided by NeutrAvidin™-FITC, the biotinylated secondary antibody, and the primary antibody. When the primary antibody was omitted, there was a reduced Raman signal (Fig. 4d) suggesting a minor amount of non-specific binding. Fig. 4e shows a Raman spectrum obtained from a high intensity area in the confocal Raman image (Fig. 4b) in which the strong G-band signal directly confirms the presence of SWNTs. Fig. 4f shows a Raman

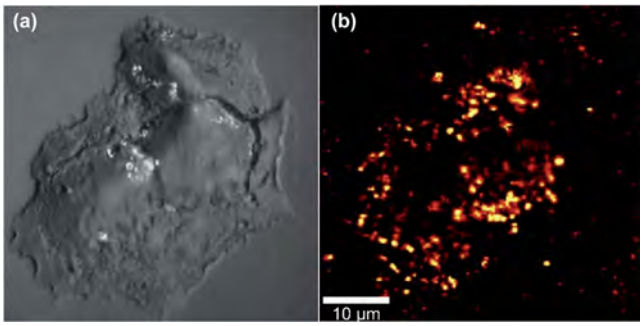

Fig. 5 Optical (a) and Raman (b) images (50 × 50 μm) of the same BT-474 cells following incubation with C-SWNTs for 3 days at 37 °C. The bright yellow areas in (b) correspond to G-band intensities (integrated from 1480–1660 cm^{-1}) acquired from each 1 μm^2 pixel in the image.

spectrum obtained from the control cells (Fig. 4d), which reflects a small amount of non-specific signal in the Raman image, in particular, the small peak at 1570–1610 cm^{-1}.

To estimate the amount of B-SWNTs bound to Her2 receptors on the BT-474 cells at 15 °C, the Raman G-band intensities measured from spectra associated with the image pixels were summed. The average Raman intensity for the specific binding of B-SWNTs to BT-474 cells at 15 °C was $1.10 \pm 0.07 \times 10^8$ CCD counts per cell as compared to $0.07 \pm 0.04 \times 10^8$ CCD counts per cell for the control sample without primary antibody. This 94% reduction in Raman signal indicates that there was minimal non-specific binding of B-SWNTs to BT-474 cells at 15 °C in the absence of the primary antibody.

Further evidence that the distribution of B-SWNTs represents targeting of Her-66 to Her2 receptors was provided by performing cell uptake studies for 3 days with non-targeted SWNTs at 37 °C, conditions under which the SWNTs are internalized by fluid-phase endocytosis and are delivered to lysosomes.[38] BT-474 cells were incubated with C-SWNTs (0.2 mg mL^{-1}) in media for 3 days at 37 °C followed by confocal Raman microscopy to image the C-SWNTs. Fig. 5 shows an optical image (Fig. 5a) and the corresponding confocal Raman image (Fig. 5b) of the same BT-474 cell cluster that had internalized C-SWNTs. The perinuclear distribution of non-targeted SWNTs (Fig. 5b) suggests that the majority of the non-targeted SWNTs are within intracellular vesicles, probably lysosomes, consistent with the long uptake time at 37 °C used in this experiment.

Conclusion

In this article, we demonstrated a carbon nanotube-based Raman-imaging immunoassay for evaluating tumor-targeting ligands. The assay used biotinylated-SWNTs as a Raman label, avidin–biotin chemistry to link the Raman label to a receptor-targeting ligand, and confocal Raman microscopy to image whole cells. Using a breast tumor cell model, we demonstrated the usefulness of the method to assess membrane receptor/ligand systems by evaluating a monoclonal antibody, Her-66, known to target overexpressed Her2 receptors. The overall approach is versatile such that one could easily study and screen other targeting antibodies such as the Her-50 and Her-81 antibodies used by Marches *et al.*,[13] and rank them in order of efficacy of targeting. Additionally, we analyzed Raman images acquired from different focal planes within a single BT-474 cell. We found that the cellular distribution of the SWNT label, which corresponds to the distribution of Her2 receptors, suggests that the targeted SWNT complexes were present on the surface of BT-474 cells. The ability to image the interaction of targeting ligands should find widespread use in elucidating mechanisms of ligand–receptor interactions towards the preclinical optimization of a variety of targeted nanotube constructs.

Acknowledgements

This work was supported by SEMATECH/Semiconductor Research Corporation (grant ERC425-042), the Human Frontier Science Program (grant #RCY0070/2005-C), DOD (grant W81XWH-08-20004), the Texas Higher Education Coordinating Board Advanced Technology Program, and the Center for Applied Biology at The University of Texas at Dallas. We also thank Ellen S. Vitetta, Radu Marches, and Pavitra Chakravarty (UT Southwestern Center for Cancer Immunobiology) for helpful discussions and the Her-66 monoclonal antibody, and Chris Gilpin (UT Southwestern Molecular and Cellular Imaging Facility) for assistance with electron microscopy.

References

1 D. E. Gerber, *Am. Fam. Physician*, 2008, **77**, 311–319.
2 Y. Yan, G. K. Such, A. P. R. Johnston, J. P. Best and F. Caruso, *ACS Nano*, 2012, **6**, 3663–3669.
3 M. Foldvari and M. Bagonluri, *Nanomedicine*, 2008, **4**, 173–200.
4 Z. Liu, S. Tabakman, K. Welsher and H. Dai, *Nano Res.*, 2009, **2**, 85–120.
5 S. R. Ji, C. Liu, B. Zhang, F. Yang, J. Xu, J. Long, C. Jin, D. L. Fu, Q. X. Ni and X. J. Yu, *Biochim. Biophys. Acta, Rev. Cancer*, 2010, **1806**, 29–35.
6 C. Fabbro, H. Ali-Boucetta, T. Da Ros, K. Kostarelos, A. Bianco and M. Prato, *Chem. Commun.*, 2012, **48**, 3911–3926.
7 M. S. Dresselhaus, G. Dresselhaus, A. Jorio, A. G. Souza Filho and R. Saito, *Carbon*, 2002, **40**, 2043–2061.
8 R. H. Baughman, A. A. Zakhidov and W. A. de Heer, *Science*, 2002, **297**, 787–792.
9 M. Ouyang, J.-L. Huang and C. M. Lieber, *Acc. Chem. Res.*, 2002, **35**, 1018–1025.
10 P. Avouris, *Acc. Chem. Res.*, 2002, **35**, 1026–1034.
11 Y. Xiao, X. Gao, O. Taratula, S. Treado, A. Urbas, R. D. Holbrook, R. E. Cavicchi, C. T. Avedisian, S. Mitra, R. Savla, P. D. Wagner, S. Srivastava and H. He, *BMC Cancer*, 2009, **9**, 351–361.
12 R. Marches, P. Chakravarty, I. H. Musselman, P. Bajaj, R. N. Azad, P. Pantano, R. K. Draper and E. S. Vitetta, *Int. J. Cancer*, 2009, **125**, 2970–2977.

13 R. Marches, C. Mikoryak, R. Wang, P. Pantano, R. K. Draper and E. S. Vitetta, *Nanotechnology*, 2011, **22**, 095101.
14 M. A. Herrero, L. Lacerda, A. Bianco, K. Kostarelos and M. Prato, *Internet J. Nanotechnol.*, 2011, **8**, 885–897.
15 V. E. Kagan, N. V. Konduru, W. Feng, B. L. Allen, J. Conroy, Y. Volkov, I. I. Vlasova, N. A. Belikova, N. Yanamala, A. Kapralov, Y. Y. Tyurina, J. Shi, E. R. Kisin, A. R. Murray, J. Franks, D. Stolz, P. Gou, J. K. Seetharaman, B. Fadeel, A. Star and A. A. Shvedova, *Nat. Nanotechnol.*, 2010, **5**, 354–359.
16 B. Sitharaman and L. J. Wilson, *Int. J. Nanomed.*, 2006, **1**, 291–295.
17 J. H. Choi, F. T. Nguyen, P. W. Barone, D. A. Heller, A. E. Moll, D. Patel, S. A. Boppart and M. S. Strano, *Nano Lett.*, 2007, **7**, 861–867.
18 C. Cao, J. H. Kim, Y. J. Kwon, Y. J. Kim, E. S. Hwang and S. Baik, *Analyst*, 2009, **134**, 1294–1296.
19 Y. Yarden, *Oncology*, 2001, **61**, 1–13.
20 S. Ménard, E. Tagliabue, M. Campiglio and S. M. Pupa, *J. Cell. Physiol.*, 2000, **182**, 150–162.
21 C. F. Singer, W. J. Köstlerband and G. Hudelist, *Biochim. Biophys. Acta*, 2008, **1786**, 105–113.
22 L. Z. Lee, Y. Wang, H. Y. Cheng, S. Pervaiz and Y. Y. Yang, *Biomaterials*, 2009, **30**, 919–927.
23 C. I. Spiridon, M. A. Ghetie, J. Uhr, R. Marches, J. L. Li, G. L. Shen and E. S. Vitetta, *Clin. Cancer Res.*, 2002, **8**, 1720–1730.
24 C. Lamprecht, N. Gierlinger, E. Heister, B. Unterauer, B. Plochberger, M. Brameshuber, P. Hinterdorfer, S. Hild and A. Ebner, *J. Phys.: Condens. Matter*, 2011, **24**, 164206.
25 C. Zavaleta, A. de la Zerda, Z. Liu, S. Keren, Z. Cheng, M. Schipper, X. Chen, H. Dai and S. S. Gambhir, *Nano Lett.*, 2008, **8**, 2800–2805.
26 M. N. Tchoul, W. T. Ford, G. Lolli, D. E. Resasco and S. Arepalli, *Chem. Mater.*, 2007, **19**, 5765–5772.
27 H. Hu, B. Zhao, M. E. Itkis and R. C. Haddon, *J. Phys. Chem. B*, 2003, **107**, 13838–13842.
28 (*a*) P. Bajaj, M.S thesis, The University of Texas at Dallas, 2008; (*b*) P. Bajaj, Ph.D. Dissertation, The University of Texas at Dallas, 2010.
29 L. A. Nagahara, K. Hashimoto and A. Fujishima, *J. Vac. Sci. Technol., B: Microelectron. Nanometer Struct.–Process., Meas., Phenom.*, 1994, **12**, 1694–1697.
30 V. Z. Poenitzsch and I. H. Musselman, *Microsc. Microanal.*, 2006, **2**, 221–227.
31 R. Wang, C. Mikoryak, E. Chen, S. Li, P. Pantano and R. K. Draper, *Anal. Chem.*, 2009, **15**, 2944–2952.
32 M. J. O'Connell, S. M. Bachilo, C. B. Huffman, V. C. Moore, M. S. Strano, E. H. Haroz, K. L. Rialon, P. J. Boul, W. H. Noon, C. Kittrell, J. Ma, R. H. Hauge, R. B. Weisman and R. E. Smalley, *Science*, 2002, **297**, 593–596.
33 M. E. Itkis, S. Niyogi, M. E. Meng, M. A. Hamon, H. Hu and R. C. Haddon, *Nano Lett.*, 2002, **2**, 155–159.
34 A. Hartschuh, H. N. Pedrosa, J. Peterson, L. Huang, P. Anger, H. Qian, A. J. Meixner, M. Steiner, L. Novotny and T. D. Krauss, *ChemPhysChem*, 2005, **6**, 1–6.
35 J. L. Bahr and J. M. Tour, *J. Mater. Chem.*, 2002, **12**, 1952–1958.
36 C. A. Dyke and J. M. Tour, *Chem.–Eur. J.*, 2004, **10**, 812–817.
37 B. Zhao, M. E. Itkis, S. Niyogi, H. Hu, J. Zhang and R. C. Haddon, *J. Phys. Chem. B*, 2004, **108**, 8136–8141.
38 R. Wang, C. Mikoryak, S. Li, D. Bushdiecker II, I. H. Musselman, P. Pantano and R. K. Draper, *Mol. Pharmaceutics*, 2011, **8**, 1351–1361.